JOURNAL OF SPACECRAFT AND ROCKETS
Vol. 40, No. 3, May–June 2003

Numerical Investigation of Canard-Controlled Missile with Planar and Grid Fins

James DeSpirito*
U.S. Army Research Laboratory, Aberdeen Proving Ground, Maryland 21005-5066
and
Milton E. Vaughn Jr.† and W. David Washington‡
U.S. Army Aviation and Missile Research, Development, and Engineering Center, Redstone Arsenal, Alabama 35898-5000

Viscous computational fluid dynamic simulations were used to predict the aerodynamic coefficients and flowfield around a generic canard-controlled missile configuration in supersonic flow. Computations were performed at Mach 1.5 and 3.0, six angles of attack between 0 and 10 deg, with 0- and 10-deg canard deflection, and with planar and grid tail fins, for a total of 48 cases. Validation of the computed results was demonstrated by the very good agreement between the computed aerodynamic coefficients and those obtained from wind-tunnel measurements. Visualizations of the flowfield showed that the downwash off of the canards produced a low-pressure region on the starboard side of the missile that, in turn, produced an adverse side force. The pressure differential on the leeward fin produced by the interaction with the canard trailing vortices is primarily responsible for the adverse roll effect observed when planar fins are used. Grid tail fins improved the roll effectiveness of the canards at low supersonic speed. Flow visualizations from the simulations performed in this study help in the understanding of the flow physics and can lead to improved canard and tail fin designs for missiles and rockets.

Nomenclature

A	=	cell face area, m^2
C_l	=	rolling moment coefficient
C_m	=	pitching moment coefficient
C_n	=	yawing moment coefficient
C_p	=	pressure coefficient
C_x	=	axial force coefficient
C_y	=	side force coefficient
C_z	=	normal force coefficient
D	=	missile base diameter, m
E	=	total energy, J
$\boldsymbol{F}$	=	inviscid flux vector
$\boldsymbol{G}$	=	viscous flux vector
$\boldsymbol{H}$	=	vector of source terms
$\boldsymbol{i}$, $\boldsymbol{j}$, and $\boldsymbol{k}$	=	Cartesian unit vectors
M	=	Mach number
p	=	pressure, N/m^2
$\boldsymbol{q}$	=	heat flux vector
u, v, and w	=	velocity components in x, y, and z directions, m/s
V	=	cell volume, m^3
$\boldsymbol{v}$	=	velocity vector ($= u\boldsymbol{i} + v\boldsymbol{j} + w\boldsymbol{k}$)
$\boldsymbol{W}$	=	vector of conservative variables
x, y, and z	=	axial, horizontal, and vertical body axes
α	=	angle of attack, deg
δ	=	canard deflection angle, deg
ν	=	kinematic viscosity, m^2/s
ρ	=	density, kg/m^3
$\boldsymbol{\tau}$	=	viscous stress tensor

Received 8 July 2002; presented as Paper 2002-4509 at the Atmospheric Flight Mechanics Conference, Monterey, CA, 5–8 August 2002; revision received 17 February 2003; accepted for publication 25 February 2003.

*Aerospace Engineer, Weapons and Materials Research Directorate, Ballistics and Weapons Concepts Division, AMSRL-WM-BC. Senior Member AIAA.

†Aerospace Engineer, Aerodynamics Technology Department, AMSAM-RD-SS-AT. Senior Member AIAA.

‡Aerospace Engineer, Aerodynamics Technology Department, AMSAM-RD-SS-AT; currently Aerospace Engineer, Missile Systems Department, Dynetics, Inc., Huntsville, AL 35814. Senior Member AIAA.

Introduction

MISSILE concepts with forward control fins, or canards, have been used for many years. However, previous studies have shown that concepts with canards can suffer from adverse induced rolling moments.[1–4] One method used to alleviate this problem is to allow the tail fins to spin, decoupling the torque generated on the fin assembly from the missile body. However, this method does add some system complexity and weight. The use of grid fins, or "lattice controls," for the tail control surfaces instead of conventional planar fins was recently proposed by the authors from the U.S. Army Aviation and Missile Research, Development, and Engineering Center (AMRDEC) as a possible remedy for the roll control problems.

A grid fin is an unconventional lifting and control surface that consists of an outer frame supporting an inner grid of intersecting planar surfaces of small chord. The aerodynamics of grid fins have been investigated since 1985 by AMRDEC.[5–7] Studies have shown that when compared to conventional planar fins, grid fins have advantages such as effective aerodynamic control at high α and high Mach number, a small hinge moment, compact storage, improved yaw stability, and attenuated body–vortex interference.[5,6,8] The primary disadvantage of the grid fin concept is a higher drag than conventional planar fins, which can be minimized with the proper design.[7] Computational fluid dynamic (CFD) techniques to calculate the viscous flow around grid fins were recently demonstrated.[9,10]

In the present study, the CFD techniques demonstrated previously[9,10] were applied to study the roll control effectiveness of both planar and grid fins on a generic canard-controlled missile shape. The numerical calculations were validated with wind-tunnel data from an experimental study performed by AMRDEC and the former Defence Research Establishment Valcartier (DREV), now the Defence Research and Development Canada—Valcartier. The objectives of the CFD study were to provide insight into the fluid dynamic phenomena that 1) cause roll reversal on canard-controlled missiles with planar tail fins and 2) permit the retention of roll control when grid tail fins are used on canard-controlled missiles. The CFD simulations provide visualizations of the flowfield that aid in

the understanding of the flow physics responsible for the adverse forces and moments observed in the wind-tunnel and calculated results.

Computational Approach

Geometry and Simulation Parameters

The investigation used CFD to determine the flowfield and aerodynamic coefficients on a 16-caliber, four-finned, generic canard-controlled missile. This study followed the experimental wind-tunnel investigation performed at DREV. The DREV wind tunnel is an intermittent, in-draft wind tunnel with a 0.6×0.6 m test section. In this type of tunnel, the air flows from an atmospheric pressure tank to a vacuum tank, and the Reynolds number is lower than free-flight values at high Mach numbers. The wind-tunnel Reynolds number ranges from about 1.56×10^7 m^{-1} at $M = 1.15$ to 4.7×10^6 m^{-1} at $M = 4.0$.

The geometry used in the CFD study was that of the wind-tunnel models. Four canards on the ogive were in line with the fins. Two fin types were investigated: conventional planar fins and grid fins. Figures 1 and 2 show the geometry for the planar fin and grid fin cases, respectively. The missile was 16 caliber long with a hemispherical nose on a 3.7-caliber truncated tangent ogive. The canard midchord was located 0.96 caliber from the missile nose, and the fin midchord was located 1.5 caliber from the missile base. The canards (Fig. 3a) were a double-wedge design, with a trapezoidal planform and a span of 0.37 caliber, a root chord of 0.36 caliber, a tip chord of 0.13 caliber, a midchord root thickness of 0.03 caliber, and a taper ratio of 1.48. The planar fins were a double-wedge design, with a rectangular planform and a span of 0.78 caliber, a chord of 0.65 caliber, and a mid-chord thickness of 0.03 caliber. The grid fins (Fig. 3b) consisted of 23 cubic and 12 prismatic cells with a span of 0.74 caliber, a chord of 0.10 caliber, and a thickness of 0.46 caliber. The web thickness between the grid fin cells was 0.003 caliber.

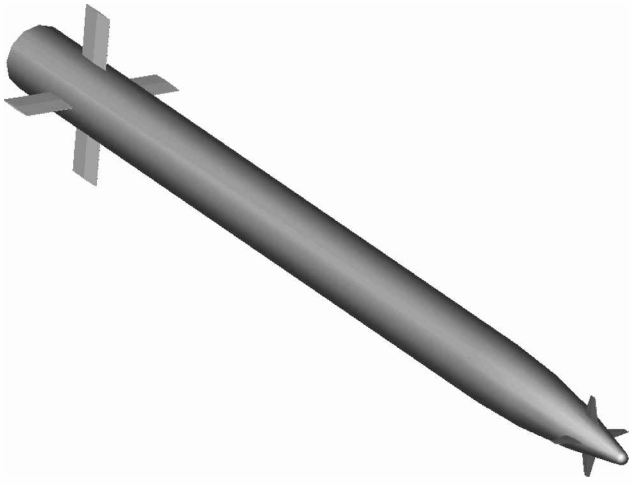

Fig. 1 Generic canard-controlled missile with planar fins.

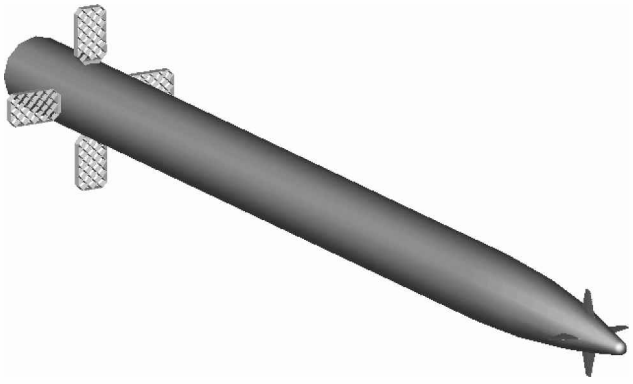

Fig. 2 Generic canard-controlled missile with grid fins.

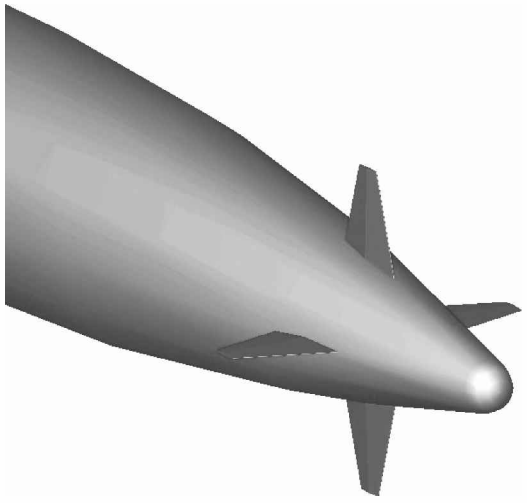

Fig. 3a Missile nose with canards at 0-deg deflection.

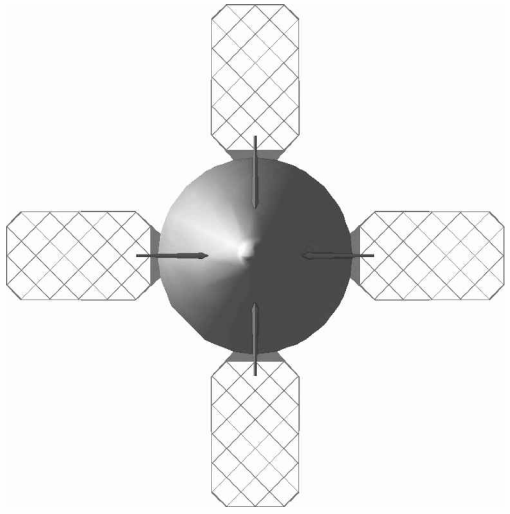

Fig. 3b Front view of missile.

The analyses were performed at two Mach numbers, $M = 1.5$ and 3.0; two canard deflections, $\delta = 0$ and 10 deg; and at six angles of attack, $\alpha = 0$, 2, 4, 6, 8, and 10 deg. The DREV wind-tunnel conditions were used in this study. For $M = 1.5$, the freestream conditions were a Reynolds number of 1.4×10^7 m^{-1}, a static temperature of 206 K, and a static pressure of 2.6×10^4 Pa. For $M = 3$, the freestream Reynolds number was 7.6×10^6 m^{-1}, the static temperature was 107 K, and the static pressure was 2.77×10^3 Pa. The model reference diameter D was 30 mm, and the moment reference point was 10.63 caliber aft of the missile nose. The simulations were performed with the missile in the cruciform + configuration. The DREV wind-tunnel data ranged from -4 to $+15$ deg angle of attack. In the $\delta = 10$ deg case, all four canards were deflected in the same direction, intended to give a positive roll, which was defined as clockwise when viewed from the rear of the missile.

Solver

Steady-state calculations were used to compute the flowfield by the use of the commercial CFD code, FLUENT, Version 5.5. The implicit, compressible (coupled), unstructured-mesh solver was used. The second-order spatial descritization equations were used. The three-dimensional, time-dependent, Reynolds-averaged Navier–Stokes equations are solved with the finite volume method:

$$\frac{\partial}{\partial t}\int_V \boldsymbol{W}\mathrm{d}V + \oint [\boldsymbol{F} - \boldsymbol{G}]\cdot \mathrm{d}\boldsymbol{A} = \int_V \boldsymbol{H}\mathrm{d}V \qquad (1)$$

where

$$\boldsymbol{W} = \begin{Bmatrix} \rho \\ \rho u \\ \rho v \\ \rho w \\ \rho E \end{Bmatrix}, \qquad \boldsymbol{F} = \begin{Bmatrix} \rho \boldsymbol{v} \\ \rho \boldsymbol{v} u + p\boldsymbol{i} \\ \rho \boldsymbol{v} v + p\boldsymbol{j} \\ \rho \boldsymbol{v} w + p\boldsymbol{k} \\ \rho \boldsymbol{v} E + p\boldsymbol{v} \end{Bmatrix}, \qquad \boldsymbol{G} = \begin{Bmatrix} 0 \\ \tau_{xi} \\ \tau_{yi} \\ \tau_{zi} \\ \tau_{ij} v_j + \boldsymbol{q} \end{Bmatrix} \tag{2}$$

$\boldsymbol{F}$ is evaluated by a standard upwind flux-difference splitting. In the implicit solver, each equation in the coupled set of governing equations is linearized implicitly with respect to all dependent variables in the set, resulting in a block system of equations. A block Gauss–Seidel, point implicit linear equation solver is used with an algebraic multigrid method to solve the resultant block system of equations. The coupled set of governing equations is discretized in time, and time marching proceeds until a steady-state solution is reached. In the implicit scheme, which was used in this study, an Euler implicit discretization in time is combined with a Newton-type linearization of the fluxes.

A modified form of the k–ε two-equation turbulence model was used in this study. Called the "realizable" k–ε model in FLUENT, it differs from the standard k–ε model in that it contains a new formulation for the turbulent viscosity and a new transport equation for the dissipation rate. This equation was derived from an exact equation for the transport of the mean-square vorticity fluctuation.[11] The term realizable means that the model satisfies certain mathematical constraints on the Reynolds stresses consistent with turbulent flow physics. The realizable k–ε model has shown substantial improvements over the standard k–ε model, where flow features include strong streamline curvature, vortices, and rotation.[11]

Computational Mesh and Boundary Conditions

The geometry and unstructured mesh were generated using the preprocessor, GAMBIT, supplied in the FLUENT software suite. Canard deflection and angle of attack precluded the use of symmetry or periodicity, and so a full three-dimensional mesh was required. In generation of the meshes, boundary-layer mesh spacing was used near the missile body and fin surfaces. The two-layer zonal model was used for the near-wall equations, and the first point off of the surface (cell center) was about 7.0×10^{-5} caliber from the surface, chosen to give a y^+ value of about 1.0. The mesh stretching ratio was kept below 1.25. About 144 cells were used on the missile body in the circumferential direction, with this value increased in the grid fin region.

An all-hexahedral (hex) mesh was used for the planar fin case, with a total number of cells of about 4.9×10^6. O-grid-type meshes were generated around the canards and planar fins. Figures 4a and 4b show the surface mesh in the tail region and ogive region, respectively. A hybrid hex and tetrahedral (tet) mesh was used for the grid fin case, with a total number of cells of about 1.57×10^7. The first 13 caliber of the missile was meshed with the same type hex mesh as in the planar fin case. A tet mesh was used in the tail region (Fig. 4c) to mesh the complicated grid fin structure. Layers of triangular prisms were used on the body to capture the boundary layer (Fig. 4d). The tet mesh in the tail is matched to the forward hex mesh via a layer of pyramidal cells. Because of meshing constraints, prism layers were not used around the grid fins, and so the spacing of the first point off of the grid fin surfaces was larger than optimum. Postprocessing

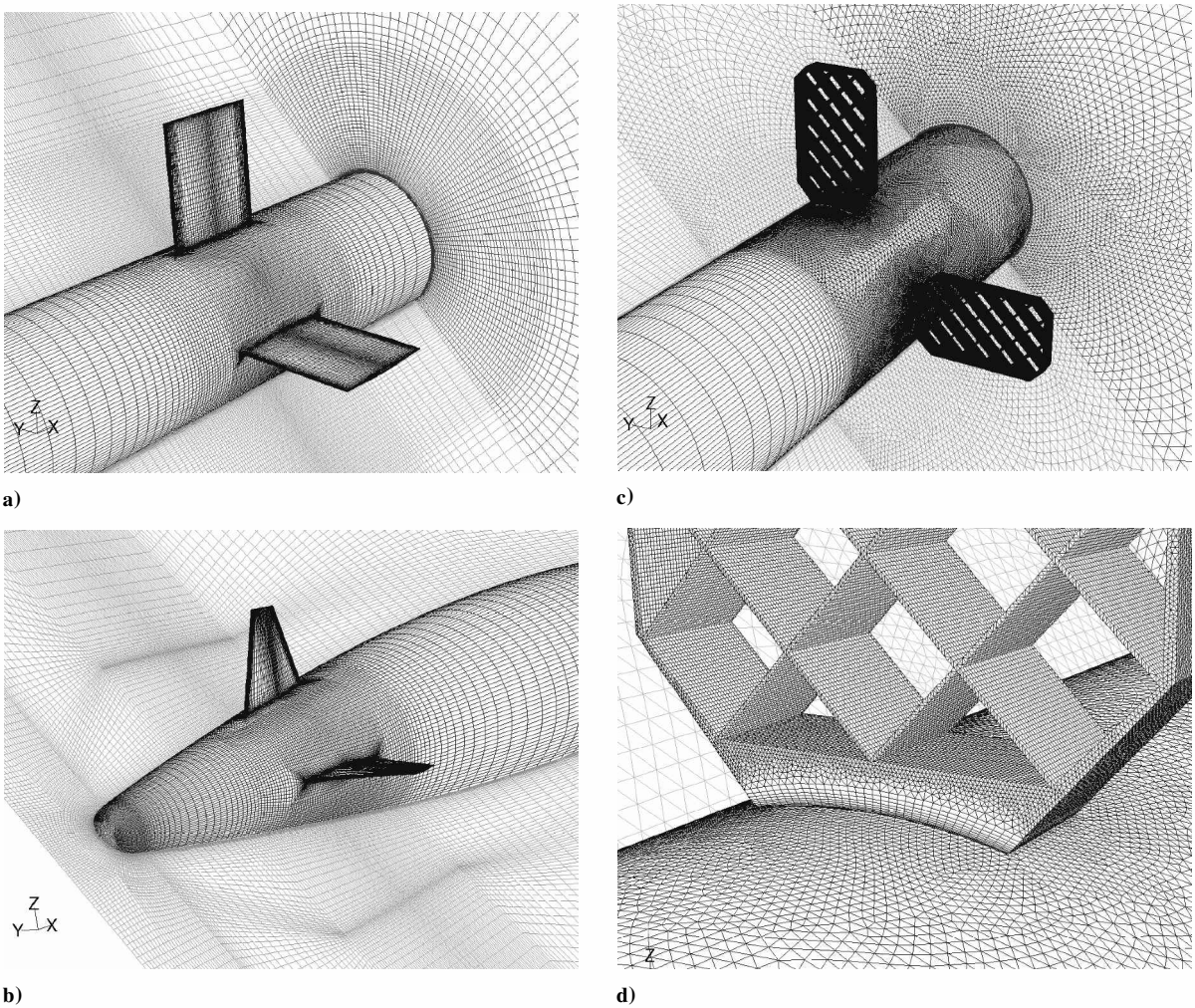

Fig. 4 Views of computational mesh: a) tail region of planar fin case, b) ogive region, c) tail region of grid fin case, and d) close-up of grid fin base.

of the runs showed that the y^+ value on the missile body, canards, and planar fins were less than 1.0. The y^+ value on the grid fins ranged from about 2 to 15, with most of the grid fin surface near the higher value. These values are not optimum for calculation of the boundary-layer properties on the grid fins, and this must be considered when the fin forces are examined, especially the axial force.

The base flow was not simulated in these calculations, and so the mesh ended at the base of the missile. For supersonic flow, this has been found to be a reasonable methodology, especially if any tail fin surfaces are not located too close to the base of the missile. The computational domain extended about 4 caliber from the missile body. A pressure-outlet boundary condition was used downstream, a pressure-inlet (with freestream conditions) boundary condition was used upstream, and a pressure-far-field boundary condition was used for the outer boundary. A nonslip wall boundary condition was used for all solid surfaces.

Solution Methodology

The simulations were performed in parallel on Silicon Graphics Origin 2000 and 3800 machines. The simulations were run with a maximum Courant–Friedrichs–Lewy (CFL) number of 10 for the planar fin cases and 5 for the grid fin cases. Each case was started with a lower CFL value (usually about 1.0) and ramped up to the maximum during the first few hundred iterations of the simulation. The calculations took about 300–600 μs/cell/iteration of CPU time, using 28 processors for the planar case and 64 or 96 processors for the grid fin case. For example, it took about 74–148 s of CPU time per iteration to solve the grid fin case with 64 processors. Convergence was determined by tracking the changes in the flow residuals and the aerodynamic coefficients during the solution. The solution was deemed converged when the flow residuals had stabilized and the aerodynamic coefficients were changing less than 0.5% after the last 100 iterations. The aerodynamic coefficients converged in about 1000–1500 iterations. The residuals dropped between three and four orders of magnitude in the $M = 1.5$ cases and between two and three orders of magnitude in the $M = 3.0$ cases.

The planar fin cases were run with the double-precision solver. To reduce the computer memory required, the grid fin cases were run with the single-precision solver. A planar fin case ($\alpha = 4$ deg, $\delta = 10$ deg) was first repeated with the single-precision solver to determine whether there was an effect on the calculated solution. The six aerodynamic coefficients calculated with the single precision solver were within 0.5% of those calculated with the double-precision solver. Four of the coefficients were within 0.1%. Therefore, the single-precision solver was adequate for these computations.

Mesh adaption was used to determine mesh independence. The mesh for two planar fin cases ($\alpha = 4$ and 10 deg; both at $\delta = 10$ deg) were adapted on the static pressure gradient with the adaption tools in the FLUENT software. After adaption, the cases were again run until convergence was achieved. The mesh size increased by 22% for the $\alpha = 4$ deg case and by 13% for the $\alpha = 10$ deg case. The maximum change in the aerodynamic coefficients was 0.9% for the $\alpha = 4$ deg case, with four of the six coefficients changing less than 0.5%. The coefficients changed less than 0.2% after mesh adaption in the $\alpha = 10$ deg case. These results show that the original mesh used for the planar fin case had high enough resolution for a mesh-independent solution. For the grid fin case, the mesh on the first 13 caliber is the same as the planar fin case, and so it is also adequate. In the tail region, the small cell sizes required for the grid fin surfaces resulted in a volume mesh that should have had more than adequate resolution, and so no mesh adaption was performed.

Results and Discussion

Aerodynamic Coefficients

The viscous and pressure forces from the computed flowfields were integrated along the missile body, canard, and fin surfaces to calculate the aerodynamic coefficients. The axial force, normal force, side force, rolling moment, pitching moment, and yawing moment are presented in missile-based coordinates. The coordinate system is right handed, with the x axis coinciding with the missile axis and oriented to the rear, the y axis oriented to the missile's starboard side, and the z axis oriented upward. The forces are positive when they coincide with the positive coordinate axes. The rolling moment is positive when the roll is clockwise when looked at forward from the aft end of the missile. The yawing moment is positive when the nose moves right and the pitching moment is positive when the nose moves upward. The reference area is the cross-sectional area of the missile base and the reference length is the diameter of the missile. Because the base flow was not calculated, only the forebody axial force is compared to the data. The forebody axial force from the experimental data was obtained by correction of the measured total axial force for the base drag component by the use of measured pressures at the base of the wind-tunnel model. Not including the base flow in the simulations can result in errors of a few percent in the computed forebody axial force, whereas use of localized base pressure measurements to obtain the experimental forebody axial force correctly can also lead to errors of a few percent.[9]

All of the computed aerodynamic coefficients showed very good agreement with experimental values from the DREV wind tunnel. The computed and measured normal force and pitching moment coefficients for the $M = 1.5$ planar fin case are compared in Figs. 5 and 6, respectively. Also shown in Figs. 5 and 6 are the predictions from the AP98 aeroprediction code.[12] AP98 is an engineering code based on empirical and theoretical methods. However, AP98 cannot predict rolling moments or side forces and does not have the capability to model grid fins, and so comparisons are made only where applicable. The comparison of the CFD and AP98 predictions is excellent. The difference between the predicted and measured values increases with α. The differences are 14% for C_z and 20% for C_m at

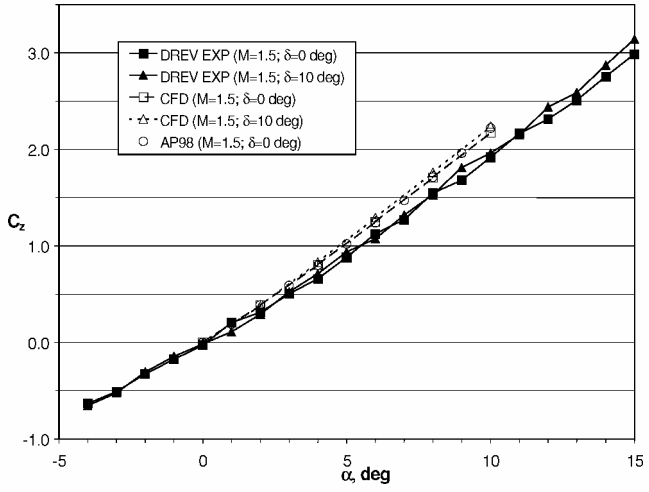

Fig. 5 Normal force coefficient, planar fin case, $M = 1.5$.

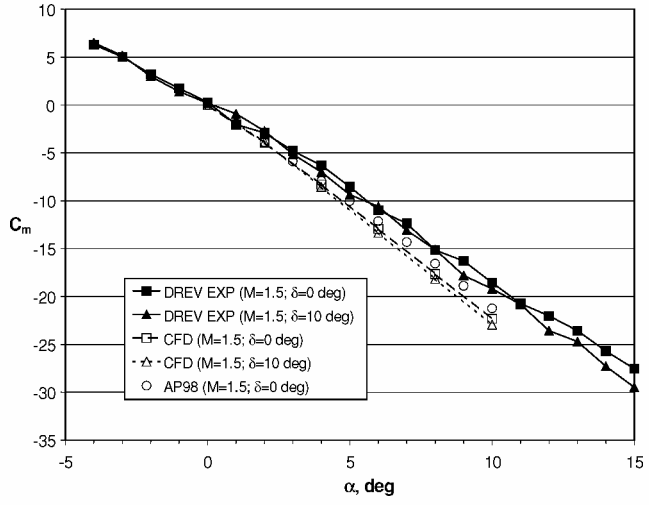

Fig. 6 Pitching moment coefficient about nose, planar fin case, $M = 1.5$.

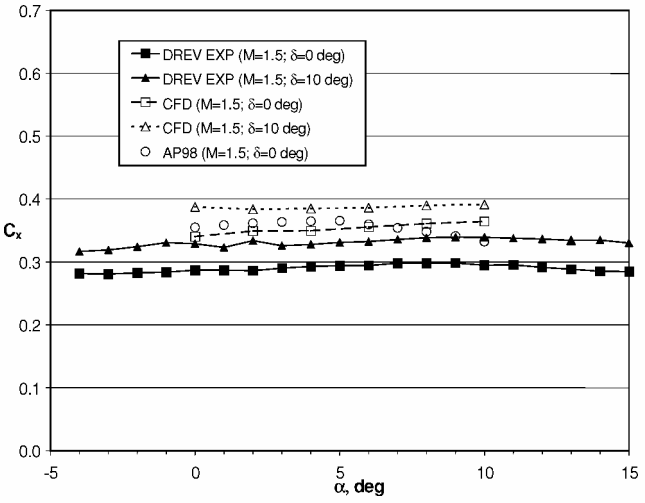

Fig. 7 Axial force coefficient, planar fin case, $M = 1.5$.

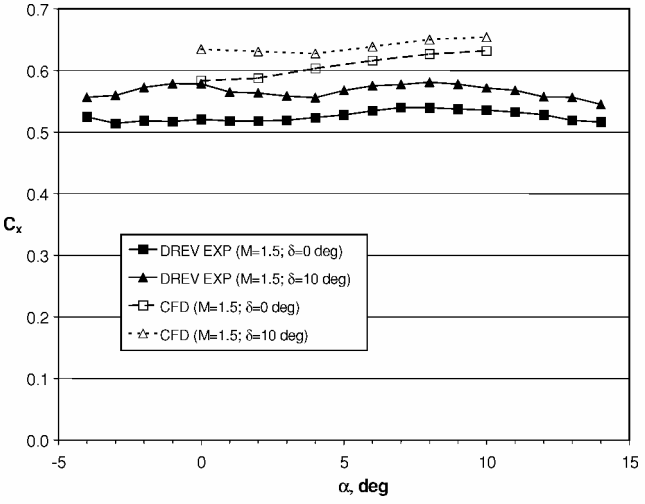

Fig. 8 Axial force coefficient, grid fin case, $M = 1.5$.

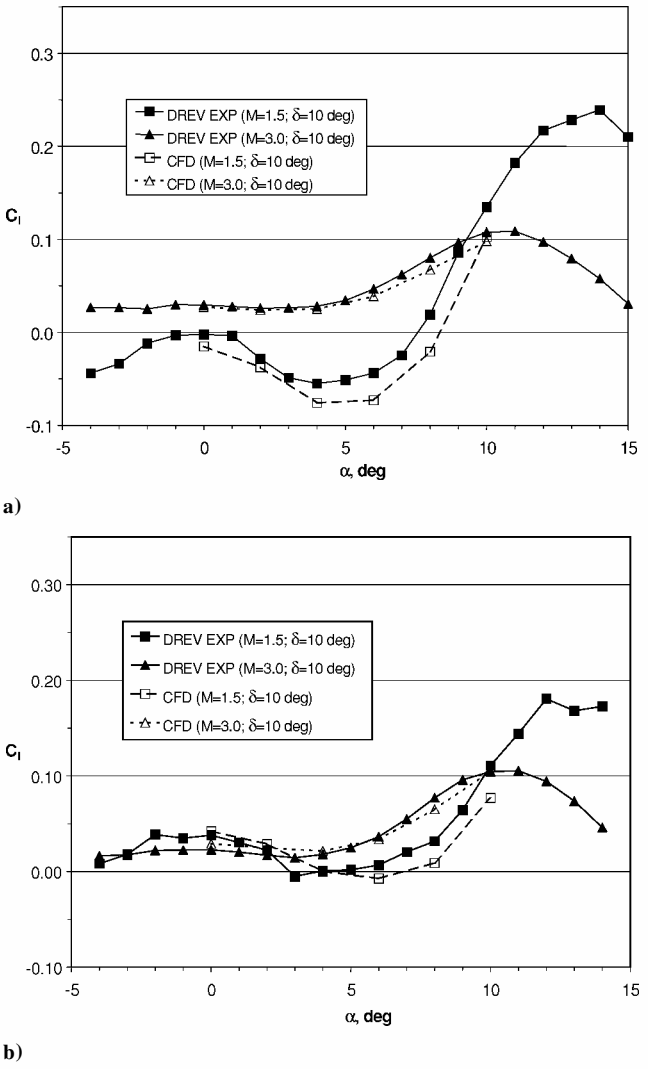

Fig. 9 Rolling moment coefficient for a) planar fin case and b) grid fin case.

$\alpha = 10$ deg. In general, the slope of the linear portion of the curve is steeper in the predicted case. However, the predicted trend is the same as the measured trend, including the increased curvature at the higher Mach number. Similar results were obtained for both the $M = 3.0$ and the grid fin cases, which are not shown here for space limitations, but are presented in a final report.[13]

The computed and measured axial force coefficients for the $M = 1.5$ planar and grid fin cases are compared in Figs. 7 and 8, respectively. Again, the CFD and AP98 predictions compare very well. The comparison with the wind-tunnel data is not as good, with the difference between the predicted and measured C_x values ranging from about 7.5 to 15%, but it is still considered acceptable. Part of this difference is likely due to the combined errors associated with the experimental base pressure measurement and the lack of a base flow in the CFD simulation.[9] The forebody C_x for the grid fin case is about 1.7 times that observed in the planar fin case. Note that the drag of the grid fins on this model is larger than could be achieved in an optimum design. First, the grid fin frame is not chamfered, which has been shown to reduce the fin drag dramatically.[7] Second, because of the small size of the wind-tunnel model, the web thickness could not be scaled down to the proper design thickness due to machining limitations, and it is about 1.5 times larger than optimum. The fin drag has been shown to be directly related to the thickness of the webs and the number of webs present.[14] Earlier studies,[8,9] with an optimum web thickness and chamfered grid fin frame showed an increase in forebody C_x for a grid finned missile of only 1.4 times that of a planar finned missile.

An important objective of this study was to predict accurately the induced roll moment and side force observed in the wind-tunnel experiments. Validation of these components gives confidence in the flow visualizations obtained from the CFD. As shown in Fig. 9, very good agreement between the computed and experimental values of the rolling moment coefficient was obtained. The experimental C_l had a large amount of bias. This bias was removed for the $\delta = 10$ deg case shown in Fig. 9 by the use of a method that DREV uses, which is as follows. The C_l for the $\delta = 0$ deg case, which should be zero at all α, but that was not due to a bias, is subtracted from the C_l for the $\delta = 10$ deg case. This procedure assumes that the bias is constant between test runs. A small difference between the computed and experimental C_l remains; however, note that the absolute magnitude of the C_l is small (< 0.1), so that the agreement is still quite good. The CFD accurately captured the nonlinear, adverse roll phenomenon. The agreement in the shape of the curve, including reversal of the roll moment direction in the $M = 1.5$ planar fin case (Fig. 9a), is excellent. Also note that the direction of roll moment in the $M = 1.5$ planar fin case is the opposite of that which should be induced by the deflected canards until α is above 8 deg. This effect, which appears to be due to the canard trailing vortices interacting with the planar fins, will be discussed further when the flowfield is presented. For the $M = 1.5$ grid fin case (Fig. 9b), C_l is positive at $\alpha = 0$ deg, decreasing to near zero in the range of $4 < \alpha < 7$ deg (some loss of roll control). At $M = 3.0$, C_l is always positive and is similar for both fin types.

The CFD also accurately predicted the nonlinear induced side force characteristics observed in the canard deflected cases. Figure 10 shows the comparison of the computed and measured C_y for the planar and grid fin cases at both Mach numbers and

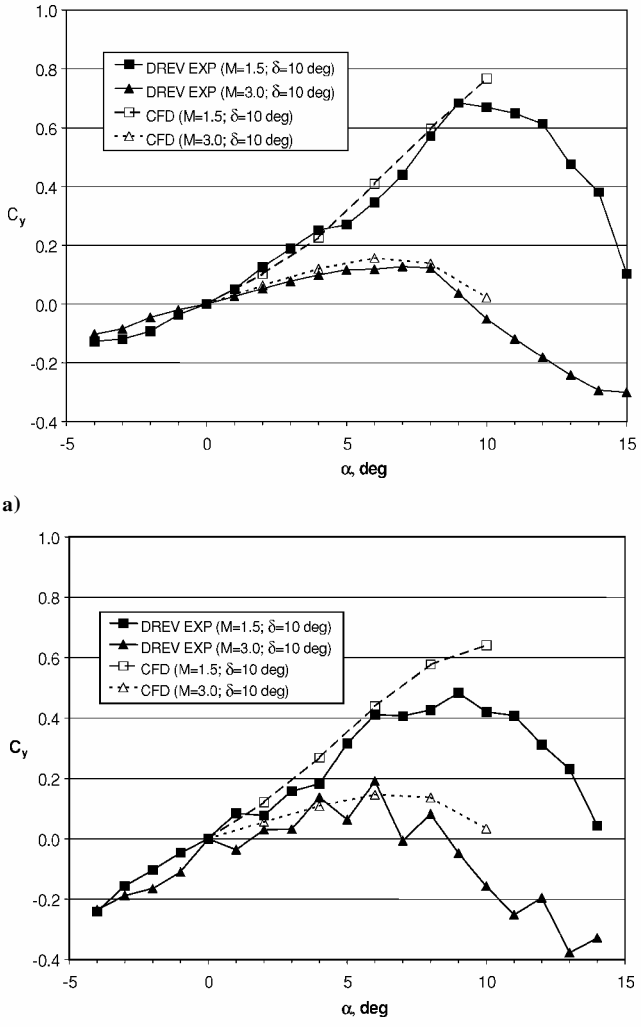

Fig. 10 Side force coefficient for a) planar fin case and b) grid fin case.

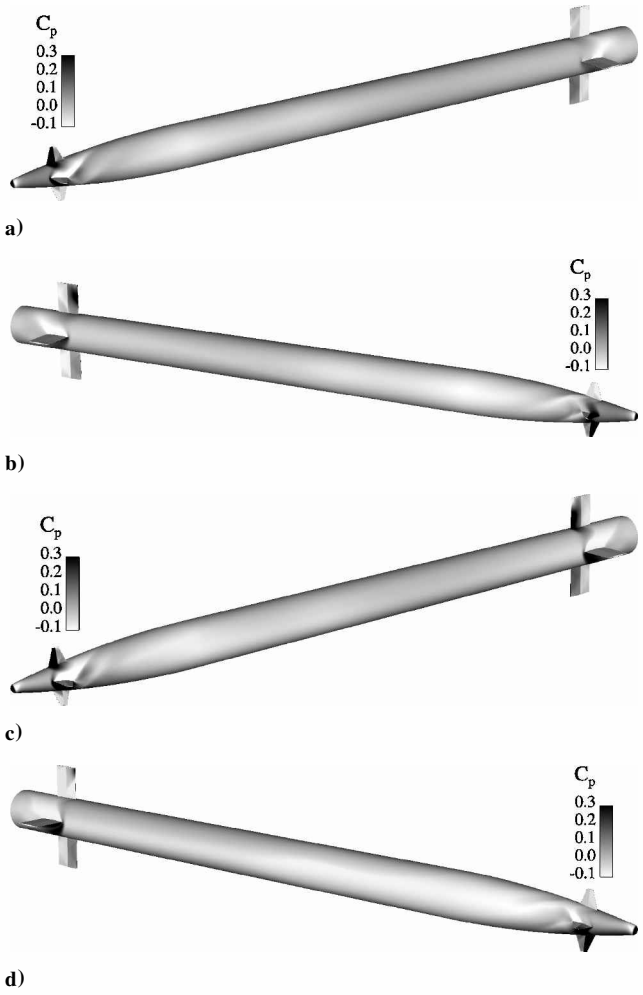

Fig. 11 Views of C_p contours at $M = 1.5$ for planar fin case: a and c) port and b and d) starboard with $\delta = 10$ deg; and a and b) $\alpha = 4$ deg and c and d) $\alpha = 10$ deg.

$\delta = 10$ deg. There was little difference in C_y due to fin type at either Mach number. At $M = 3.0$, the maximum C_y was not too large. However, at $M = 1.5$, C_y was about five times larger than at $M = 3.0$. The flow is symmetric about the vertical plane for the $\delta = 0$ deg cases. Thus, $C_y = 0$ and $C_l = 0$, and they are not shown. The change in slope of the C_y vs α curve at $M = 3.0$ is accurately predicted for both fin types. The maximum value of C_y is not predicted as well at $M = 1.5$. The simulations end near the maximum value in the $M = 1.5$ case, but it appears that the beginning of the change in slope is correctly predicted in the grid fin case (Fig. 10b).

These results show that the CFD accurately predicted the aerodynamic coefficients for a generic canard-controlled missile with both conventional planar fins and grid fins in supersonic flow. With the CFD results validated, the computed flowfield was used to investigate the physics responsible for roll reversal or loss of roll control.

Flowfield Visualizations

Visualizations of the flowfield showed that the canard deflection had a strong effect on the forces on the missile. Figure 11 shows the C_p distribution on the missile surfaces for the planar fin cases with $\delta = 10$ deg at $\alpha = 4$ and 10 deg. The $\delta = 0$ deg cases are not presented, but they showed a symmetrical C_p distribution on the missile with no contribution to C_y, C_l, or C_n. For the $\delta = 10$ deg cases, the canard trailing vortices interacted with the missile flowfield to change the pressure distribution both along the missile body and on the tail fins. The effect increases with α and is most pronounced at $M = 1.5$, where a large low-pressure region is observed on the starboard side of the missile (Figs. 11b and 11d). As α increases, the downwash off of the deflected canards generates a higher velocity and, thus, a lower pressure, on the starboard side of the missile, thereby generating the side force. Although the effect was still present at $M = 3.0$, the effect was not as large at the higher speed, which correlates with the measured C_l and C_y. The effect is also reduced after α increases past a certain value, which is shown in Fig. 10 by the reduction in C_l after the maximum is attained.

The canard deflection should give the missile a clockwise (when viewed from rear), or positive, rolling moment. At $M = 1.5$, the C_l is actually negative until $\alpha > 8$ deg. This adverse roll can be explained by examination of the pressure distribution and forces on the tail fins. A high-pressure region on the starboard side of the leeward fin at $\alpha = 4$ deg can be seen in Fig. 11b. Although not shown in Fig. 11, a similar high-pressure region was also on the windward side of the starboard fin. These unbalanced pressures on the tail fins are enough to reverse the rolling moment. At $\alpha = 10$ deg, the effect is much lower, which appears to be due primarily to the vortices trailing the port and leeward canards missing the tail fins entirely. In fact, there are unbalanced forces on the leeward tail fin (Figs. 11c and 11d) that act in addition to the canard forces to induce added positive roll. Scientific visualization movies of particle traces and C_p contours indicated that the nonsymmetrical flowfield was due to a combination of the canard trailing vortices interacting with the tail fins at low α and the crossflow separation vortices on the leeward side of the missile interacting with tail fins at high α.

The impact of the interaction of the canard trailing vortices on the tail fins is related to the strength of the vortices. There was only a small effect on the missile roll control authority at $M = 3.0$, where the intensity of the trailing vortices were much lower. This is illustrated in Fig. 12, where intense vortices were observed downstream

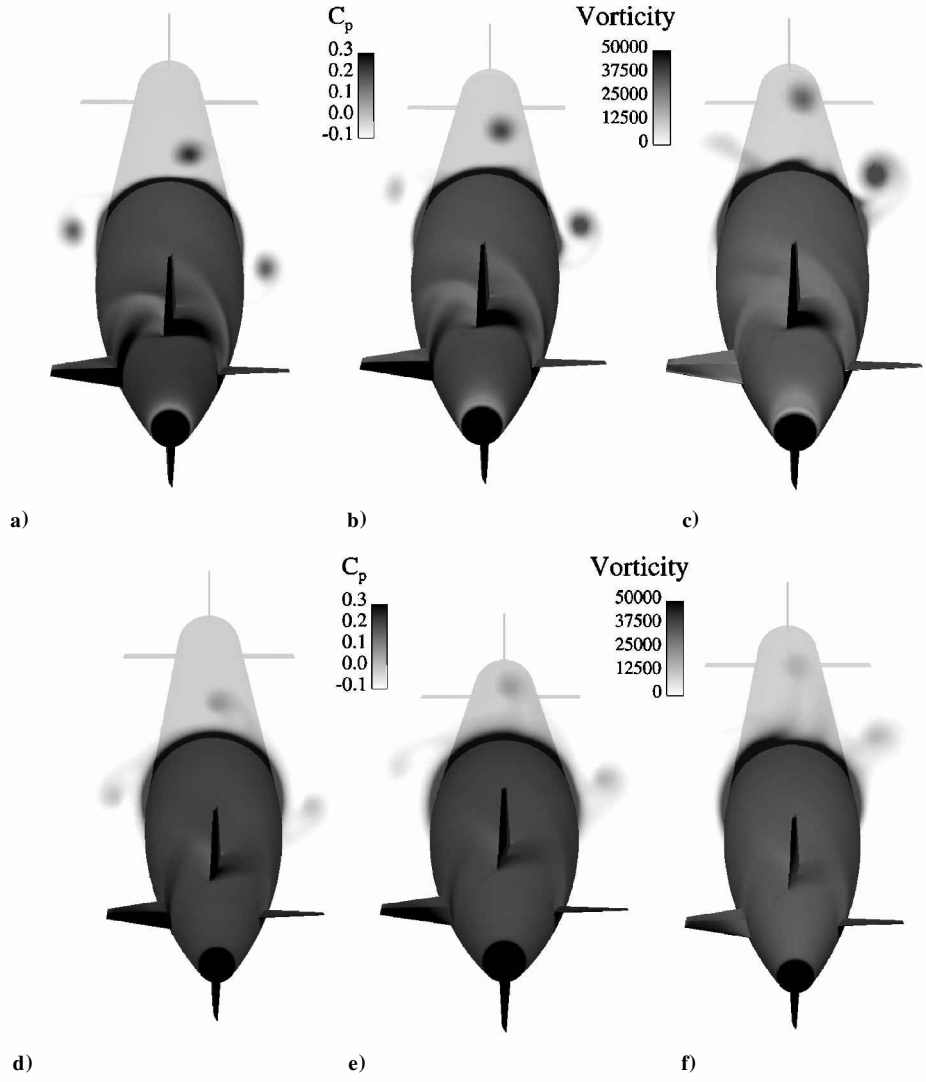

Fig. 12 C_p **contours on missile surface and vorticity contours on axial plane behind canards for** $\delta = 10$ **deg and** $\alpha = 0$**, 4, and 10 deg at a–c)** $M = 1.5$ **and d–f)** $M = 3.0$**.**

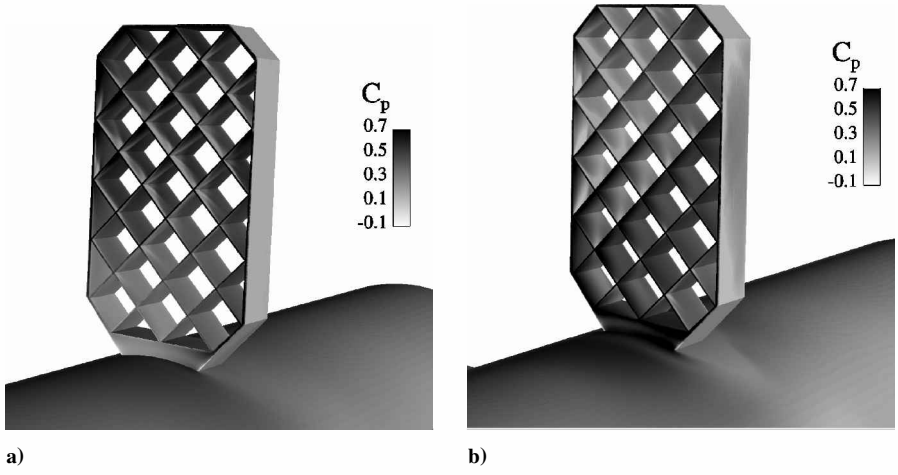

Fig. 13 C_p **contours on grid fins at** $M = 1.5$ **and a)** $\alpha = 4$ **deg and b)** $\alpha = 10$ **deg.**

of the canards at $M = 1.5$. At $M = 3.0$, the intensity of the vortices at the same axial location is much lower. At $M = 1.5$, the strength of the trailing vortices was maintained well past the tail fins.[13]

The effect in the grid fin case is more difficult to observe. In this case (Fig. 13), the induced pressure on the grid fins is distributed over the fin more than in the planar fin case. Although there was still nonuniformity in the pressure distribution on the fins, the characteristic geometry of the grid fins alleviated the unwanted rolling moment effect. At $\alpha = 0$, the unwanted rolling moment at $M = 1.5$ observed in the planar fin case is eliminated (Fig. 9). There is still a range, $4 < \alpha < 7$ deg, in which the effectiveness of the canards is severely reduced, but there is still an improvement over the planar tail fins.

These results are shown quantitatively in Fig. 14, which shows the side force coefficient on each fin for the planar and grid fin cases at $\delta = 10$ deg. In the planar fin case, the windward fin (fin 2) is at a

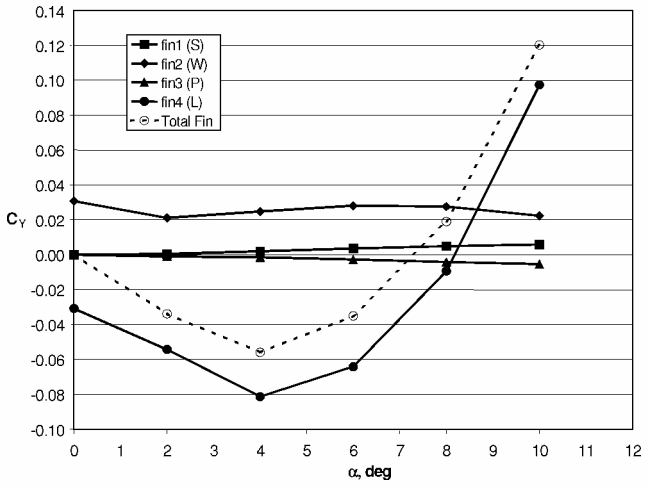

a)

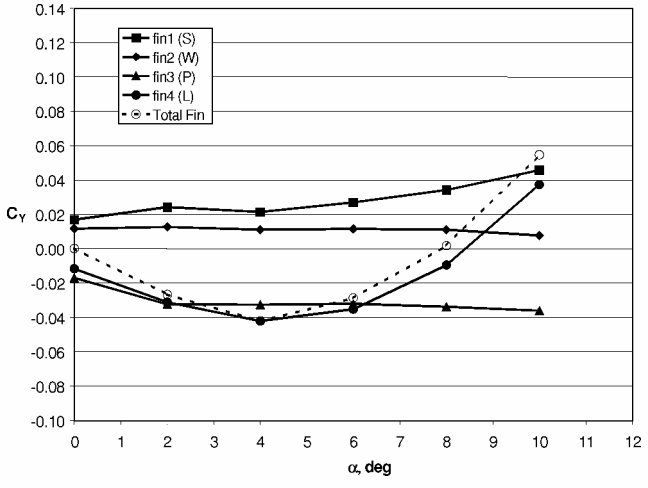

b)

Fig. 14 Side force coefficient on tail fins for a) planar fin case and b) grid fin case, for $\delta = 10$ deg.

nearly constant, small positive value. The leeward fin (fin 4) is negative until $\alpha > 8$ deg. This clearly produces the adverse roll. These force coefficients are of the same order as those on the canards,[13] but the larger moment arm of the fins produces moments larger than those produced by the canards. In the grid fin case, Fig. 14b, there are still side forces on the windward and leeward fins that tend to induce a negative roll, but this time they are lower and do not reduce the roll effectiveness of the canards as much. Also, observe that the horizontal grid fins produce a side force, unlike the planar fins. The fin side force does not affect the roll moment and only adds a very small contribution to missile side force.

The validated CFD results confirm that the use of grid tail fins dramatically improves the roll effectiveness of the canards at low supersonic speed. Visualizations of the flowfield from the simulations performed in this study help in the understanding of the flow physics and can lead to improved tail fin and canard designs.

Conclusions

Viscous CFD calculations were used to predict the aerodynamic coefficients and flowfield around a generic canard-controlled missile configuration in supersonic flow. Validation of the computed results was demonstrated by the very good agreement between the computed aerodynamic coefficients and those obtained from wind-tunnel measurements.

Visualizations of the flowfield at low supersonic speed showed that the downwash off of the canards produced a low-pressure region on the starboard side of the missile that, in turn, produced an adverse induced side force. The side force was much lower at the higher supersonic speed.

The visualizations also showed that the canard trailing vortices interact with the tail fins until α is high enough so that the vortices miss the leeward fin. The pressure differential on the leeward fin produced by the interaction with the canard trailing vortices is primarily responsible for the adverse induced roll effects observed when planar fins are used.

Grid tail fins improved the roll effectiveness of the canards at low supersonic speed. There was still an uneven pressure distribution on the grid tail fins, produced by the interaction with the canard trailing vortices. However, the design of the grid fin distributes the pressure differently, so that the side forces are lower and do not produce as large a roll moment as the planar fins do.

Acknowledgments

This work was supported in part by a grant of high-performance computing time from the U.S. Department of Defense High Performance Computing Modernization program at the U.S. Army Research Laboratory Major Shared Resource Center, Aberdeen Proving Ground, Maryland. The authors thank Richard Angelini, U.S. Army Research Laboratory, for providing scientific visualizations of the flowfields, and Eric Fournier, Defence Research and Development Canada—Valcartier, for providing discussions on the wind-tunnel data.

References

[1]Allen, J. M., and Blair, A. B., Jr., "Comparison of Analytical and Experimental Supersonic Aerodynamic Characteristics of a Forward Control Missile," *Journal of Spacecraft and Rockets*, Vol. 19, No. 2, 1982, pp. 155–159.

[2]Blair, A. B., Jr., Dillon, J. L., and Watson, C. B., "Experimental Study of Tail-Span Effects on a Canard-Controlled Missile," *Journal of Spacecraft and Rockets*, Vol. 30, No. 5, 1993, pp. 635–640.

[3]Blair, A. B., Jr., "Supersonic Aerodynamic Characteristics of a Maneuvering Canard-Controlled Missile with Fixed and Free-Rolling Tail Fins," Society of Automotive Engineers, SAE Paper 90-1993, Oct. 1990.

[4]Burt, J. R., Jr., "The Effectiveness of Canards for Roll Control," U.S. Army Missile Command, TR RD-77-8, Redstone Arsenal, AL, Nov. 1976.

[5]Washington, W. D., and Miller, M. S., "Grid Fins—A New Concept for Missile Stability and Control," AIAA Paper 93-0035, Jan. 1993.

[6]Washington, W. D., and Miller, M. S., "Experimental Investigations of Grid Fin Aerodynamics: A Synopsis of Nine Wind Tunnel and Three Flight Tests," *Proceedings of the NATO RTO Applied Vehicle Technology Panel Symposium on Missile Aerodynamics*, NATO Research and Technology Organization, RTO MP-5, Neuilly-Sur-Seine Cedex, France, 1998, pp. (10-1)–(10-14).

[7]Miller, M. S., and Washington, W. D., "An Experimental Investigation of Grid Fin Drag Reduction Techniques," AIAA Paper 94-1914, June 1994.

[8]Simpson, G. M., and Sadler, A. J., "Lattice Controls: A Comparison with Conventional, Planar Fins," *Proceedings of the NATO RTO Applied Vehicle Technology Panel Symposium on Missile Aerodynamics*, NATO Research and Technology Organization, RTO-MP-5, Neuilly-Sur-Seine Cedex, France, 1998, pp. (9-1)–(9-10).

[9]DeSpirito, J., Edge, H. L., Weinacht, P., Sahu, J., and Dinavahi, S. P. G., "Computational Fluid Dynamics Analysis of a Missile with Grid Fins," *Journal of Spacecraft and Rockets*, Vol. 38, No. 5, 2001, pp. 711–718.

[10]DeSpirito, J., and Sahu, J., "Viscous CFD Calculations of Grid Fin Missile Aerodynamics in the Supersonic Flow Regime," AIAA Paper 2001-2057, Jan. 2001.

[11]*Fluent 5.0 Users Guide*, Vol. 2, Fluent, Inc., Lebanon, NH, 1998.

[12]Moore, F. G., McInville, R. M., and Hymer, T. C., "Application of the 1998 Version of the Aeroprediction Code," *Journal of Spacecraft and Rockets*, Vol. 36, No. 5, 1999, pp. 633–645.

[13]DeSpirito, J., Vaughn, M. E., Jr., Washington, W. D., "Numerical Investigation of Aerodynamics of Canard-Controlled Missile Using Planar and Grid Tail Fins, Part I: Supersonic Flow," U.S. Army Research Lab., ARL-TR-2848, Aberdeen Proving Ground, MD, Sept. 2002.

[14]Abate, G., Winchenbach, G., and Hathaway, W., "Transonic Aerodynamic and Scaling Issues for Lattice Fin Projectiles Tested in a Ballistic Range," *Proceedings of the 19th International Symposium on Ballistics*, edited by I. R. Crewther, Vol. 1, IBS 2001 Symposium Office, Thun, Switzerland, 2001, pp. 413–420.

R. M. Cummings
Associate Editor